

Stability Analysis of Thermohaline Convection With a Time-Varying Shear Flow Using the Lyapunov Method

Kalin Kochnev¹ and Chang Liu²

Abstract—This work identifies instabilities and computes the growth rate of a linear time-varying system using the Lyapunov method. The linear system describes cold fresh water on top of hot salty water with a periodically time-varying background shear flow. We employ a time-dependent weighting matrix to construct a Lyapunov function candidate, and the resulting linear matrix inequalities formulation is discretized in time using the forward Euler method. As the number of temporal discretization points increases, the growth rate predicted from the Lyapunov method or the Floquet theory will converge to the same value as that obtained from numerical simulations. We also use the Lyapunov method to analyze the instantaneous principal direction of instabilities and compare the computational resources required by the Lyapunov method, numerical simulations, and the Floquet theory.

I. INTRODUCTION

Time dependence of flow speed is widely observed in the oceanic environment, such as the internal gravity waves and inertial waves [1], [2]. Tidal currents are another source of time dependence, which are present in nearly all sub-ice-shelf observations and can significantly influence the ice melting rate [3]. The time dependence of shear flow can also induce instabilities within parameter regimes where a steady shear flow will be stable [4], [5]. For example, time-varying shear flows can interact with thermohaline convection (driven by the diffusivity difference between temperature and salinity) to induce thermohaline-shear instability [4]. This thermohaline-shear instability was shown to exist in most high-latitude ocean regions, which plays an important role in mixing and staircase formation [4].

Stability analysis can provide key insights into pattern formation and the transition to chaotic and turbulent behaviors [6], but the time dependence of background flow introduces additional challenges in stability analysis [7]. Quasi-steady assumption and eigenvalue analysis of the time-frozen base state are known to oversimplify the dynamics of a time-varying system, and thereby may miss instabilities induced by the time-dependence [8], [9]. Floquet theory [10] is a powerful tool to analyze the stability of a periodic orbit,

but it is limited to the linear time-periodic system [7]. Stability of time-varying systems can also be analyzed by numerical simulations [4], [5]. However, simulations only provide realizations of certain initial conditions to support stability analysis, but cannot formally prove the stability. For nonlinear systems, extensive simulations with random initial conditions (e.g., 100,000 simulations [11]) might be needed to fully characterize the region of attraction.

The Lyapunov method has been widely used to analyze the stability of nonlinear systems, and can be generalized to investigate the stability of time-varying (non-autonomous) systems [8], [12]. A periodic Lyapunov function is introduced to analyze a discrete-time nonlinear periodically time-varying system, which was shown to provide a larger region of attraction estimation compared with standard Lyapunov theory [13]. Moreover, stabilization of continuous-time periodic linear systems can be achieved by solving a periodic Lyapunov differential equation [14]. The Lyapunov method can also be applied to analyze the nonlinear stability (e.g., characterization of region of attraction [15]) or analyze non-periodically time-varying systems [16], which can overcome limitations of numerical simulations and Floquet theory.

This work will employ the Lyapunov method to analyze instabilities of a linear time-periodic system that describes thermohaline-shear instability [4], where cold fresh water on top of hot salty water interacts with a periodically time-varying shear flow. We will use a periodic weighting matrix $\mathbf{P}(t)$ to construct a Lyapunov function candidate $V(\psi, t) = \psi^* \mathbf{P}(t) \psi$, where ψ is the state variable, and the superscript $(\cdot)^*$ means the Hermitian of the argument. We formulate linear matrix inequalities (LMI) to obtain an upper bound of the growth rate, and the LMI is discretized in time by a forward Euler method. The resulting LMI will be coupled over time and solve the time-varying weighting matrix $\mathbf{P}(t)$ over one period. As the number of temporal discretization points increases, the growth rate predicted from the Lyapunov method or the Floquet theory converges to that obtained from numerical simulations. We also perform an eigendecomposition of the instantaneous weighting matrix $\mathbf{P}(t)$ to uncover the principal direction of thermohaline-shear instability. The computational resources requirement is also compared among the Lyapunov method, numerical simulations, and the Floquet theory.

The paper is organized as follows. Section II introduces the linear time-varying system that describes thermohaline-shear instabilities [4]. Section III presents three methods that will be used to compute growth rate, including the Lyapunov method, numerical simulations, and the Floquet

¹School of Electrical and Computer Engineering, University of Connecticut, Storrs, CT 06269, USA kalinkochnev@proton.me

²School of Mechanical, Aerospace, and Manufacturing Engineering, University of Connecticut, Storrs, CT 06269, USA chang_liu@uconn.edu

This research was supported by the University of Connecticut (UConn) Research Excellence Program (REP). K.K. acknowledges the support from the UConn Summer Undergraduate Research Fund (SURF) Awards. The computational work for this project was conducted using resources provided by the Storrs High-Performance Computing (HPC) cluster. We extend our gratitude to the UConn Storrs HPC and its team for their resources and support, which aided in achieving these results. The data and code of this paper are publicly available at <https://doi.org/10.5281/zenodo.17227640>.

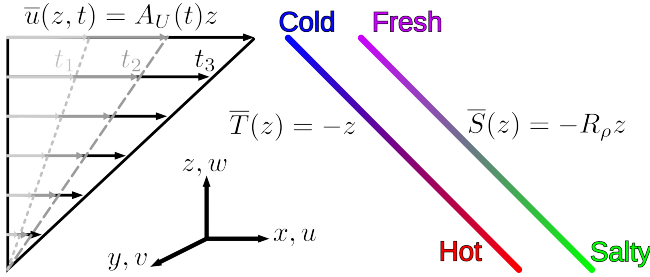


Fig. 1. The linear time-varying model analyzed here describes cold fresh water on top of hot salty water with a time-varying shear flow $\bar{u}(z, t) = A_U(t)z$, temperature $\bar{T}(z) = -z$, and salinity $\bar{S}(z) = -R_\rho z$ vary linearly over z .

theory. Section IV presents the results, and we conclude this paper with a discussion of future directions in Section V.

II. PROBLEM FORMULATION

We consider the flow configuration in Fig. 1, where we have a time-varying background shear flow $\bar{\mathbf{U}}_*(z_*, t_*) = [A_{U*}(t_*)z_*, A_{V*}(t_*)z_*, 0]^T$. We consider cold fresh water on top of hot salty water with a large-scale background temperature gradient $\partial_{z_*}\bar{T}_* < 0$ and salinity gradient $\partial_{z_*}\bar{S}_* < 0$. We assume that the density is influenced by temperature and salinity linearly $(\rho_* - \rho_{0*})/\rho_{0*} = \beta(S_* - S_{0*}) - \alpha(T_* - T_{0*})$, where α and β are expansion and contraction coefficients. Here, ρ_{0*} , T_{0*} , and S_{0*} are reference density, temperature, and salinity, respectively. We define dimensionless length, time, velocity, and pressure as $z = z_*/d$, $t = t_*/(d^2/\kappa_T)$, $u = u_*/(\kappa_T/d)$, and $p = p_*/(\rho_{0*}\nu\kappa_T/d^2)$ [4], where $d := [\kappa_T\nu/(ga|\partial_{z_*}\bar{T}_*|)]^{1/4}$, κ_T is the thermal diffusivity, and ν is the viscosity. We normalize temperature and salinity by $T = T_*/(d|\partial_{z_*}\bar{T}_*|)$ and $S = \beta S_*/(\alpha d|\partial_{z_*}\bar{T}_*|)$, and then we have dimensionless background temperature as $\bar{T} = -z$ and background salinity as $\bar{S} = -R_\rho z$. After linearization around the base state $(\bar{T}, \bar{S}, \bar{\mathbf{U}})$, we have the non-dimensional governing equation of fluctuations (T, S, \mathbf{u})

[4] as:

$$\partial_t T + \bar{\mathbf{U}} \cdot \nabla T - w = \nabla^2 T, \quad (1a)$$

$$\partial_t S + \bar{\mathbf{U}} \cdot \nabla S - R_\rho w = \tau \nabla^2 S, \quad (1b)$$

$$\partial_t \mathbf{u} + \bar{\mathbf{U}} \cdot \nabla \mathbf{u} + \mathbf{u} \cdot \nabla \bar{\mathbf{U}} = \text{Pr}[-\nabla p + \nabla^2 \mathbf{u} + (T - S)\mathbf{e}_z], \quad (1c)$$

$$\nabla \cdot \mathbf{u} = 0. \quad (1d)$$

Here, we have the density ratio $R_\rho := \beta \partial_{z_*} \bar{S}_*/(\alpha \partial_{z_*} \bar{T}_*)$, the Prandtl number $\text{Pr} := \nu/\kappa_T$, and the diffusivity ratio $\tau := \kappa_S/\kappa_T$, where ν is the viscosity and κ_S is the salinity diffusivity. The unit vector in the vertical z direction is denoted as \mathbf{e}_z . Here, we consider the horizontal direction (x, y) as periodic. The dimensionless background shear flow is $\bar{\mathbf{U}}(z, t) = [\bar{u}(z, t), \bar{v}(z, t), 0]^T = [A_U(t)z, A_V(t)z, 0]^T$ with an unbounded vertical direction z , i.e., unbounded Couette flow model. Thus, we can perform the following solution ansatz [4] to eliminate the dependence on z :

$$(T, S, u, v, w) = \Re \left[\left(\hat{T}, \hat{S}, \hat{u}, \hat{v}, \hat{w} \right) e^{ikx + i ly + imz} \right], \quad (2)$$

where $\Re[\cdot]$ means the real part of the argument, k and l are respectively horizontal wavenumbers in x and y directions, and $m(t)$ is a time-varying vertical wavenumber:

$$m(t) = m_0 - B_U(t)k - B_V(t)l. \quad (3)$$

Here, m_0 is an initial vertical wavenumber, while $B_U(t)$ and $B_V(t)$ in (3) are defined as

$$B_U(t) = \int_0^t A_U(t') dt', \quad B_V(t) = \int_0^t A_V(t') dt'. \quad (4)$$

Using (2), we can convert the linearized governing equation in (1) as a linear time-varying system expressed in (5):

$$\dot{\psi} = \mathbf{A}(t)\psi, \quad (5)$$

where the state variable $\psi = [\hat{T} \quad \hat{S} \quad \hat{u} \quad \hat{v} \quad \hat{w}]^T$. The matrix $\mathbf{A}(t)$ is defined in (6) with $c(t) = k^2 + l^2 + m(t)^2$:

$$\mathbf{A}(t) = \begin{bmatrix} -c(t) & 0 & 0 & 0 & 1 \\ 0 & -\tau c(t) & 0 & 0 & R_\rho \\ \frac{-\text{Pr} km(t)}{c(t)} & \frac{\text{Pr} km(t)}{c(t)} & -\text{Pr} c(t) & 0 & \frac{2k[kA_U(t)+lA_V(t)]}{c(t)} - A_U(t) \\ \frac{-\text{Pr} lm(t)}{c(t)} & \frac{\text{Pr} lm(t)}{c(t)} & 0 & -\text{Pr} c(t) & \frac{2l[kA_U(t)+lA_V(t)]}{c(t)} - A_V(t) \\ \frac{-\text{Pr} m(t)^2}{c(t)} + \text{Pr} & \frac{\text{Pr} m(t)^2}{c(t)} - \text{Pr} & 0 & 0 & \frac{2m(t)[kA_U(t)+lA_V(t)]}{c(t)} - \text{Pr} c(t) \end{bmatrix}. \quad (6)$$

Here, we simplify this model as a two-dimensional monochromatic shear model by setting $l = A_V(t) = 0$ and $A_U(t) = A_u \cos(\omega t)$ with the shear amplitude as $A_u = \sqrt{\frac{2\text{Pr}(R_\rho - 1)}{R_i}}$ [4]. All dimensionless parameters used in this paper are summarized in Table I.

III. METHODS

In this section, we present our formulation to compute the growth rate of the linear time-varying system in (5)

using the Lyapunov method. We then show how to obtain the growth rate using numerical simulations and the Floquet theory, which will be used as a basis for the comparison with the Lyapunov method.

A. Lyapunov stability analysis

We will have the following Theorem 1 to predict an upper bound on the growth rate. Here, $(\cdot) \preceq 0$ is negative semi-definiteness, $(\cdot) \succeq 0$ is positive semi-definiteness of the

Variable	Value/Range	Description
Pr	10	Prandtl number
R_p	2.0	Density ratio
τ	0.01	Diffusivity ratio
Ri	2.0	Richardson number
ω	0.5	Oscillation frequency of background shear
k	$[-0.5, 0.5]$	Wavenumber in the x direction
l	0	Wavenumber in the y direction
m_0	$[0, 1.5]$	Initial wavenumber in the z direction
n	[400, 2000]	Temporal grid points of $\mathbf{A}(t)$ and $\mathbf{P}(t)$
T	4π	Oscillation period $T = 2\pi/\omega$
n_{samples}	126	Sample numbers for k and m_0

TABLE I. A list of the parameters used in this work.

argument, and the superscript $(\cdot)^*$ means the Hermitian of the argument.

Theorem 1: Given a linear time-varying system $\dot{\psi} = \mathbf{A}(t)\psi$ in (5). If we can find a continuously differentiable Hermitian matrix $\mathbf{P}(t) \in \mathbb{C}^{5 \times 5}$ and $\bar{\lambda}$ by solving

$$\min \bar{\lambda} \quad (7a)$$

$$\text{subject to } \mathbf{P}(t) \succeq \epsilon \mathbf{I}, \quad \epsilon > 0, \quad \forall t \in \mathbb{R}, \quad (7b)$$

$$\dot{\mathbf{P}}(t) + \mathbf{A}^*(t)\mathbf{P}(t) + \mathbf{P}(t)\mathbf{A}(t) - 2\bar{\lambda}\mathbf{P}(t) \preceq 0, \quad (7c)$$

then $\|\psi(t)\|_2 \leq Ce^{\bar{\lambda}t}\|\psi(0)\|_2$, where C is a constant.

Proof: We consider a function $V(\psi, t) = \psi^*\mathbf{P}(t)\psi$ and compute its time derivative \dot{V} as:

$$\dot{V} = \psi^*\dot{\mathbf{P}}(t)\psi + \dot{\psi}^*\mathbf{P}(t)\psi + \psi^*\mathbf{P}(t)\dot{\psi} \quad (8a)$$

$$= \psi^*[\dot{\mathbf{P}}(t) + \mathbf{A}(t)^*\mathbf{P}(t) + \mathbf{P}(t)\mathbf{A}(t)]\psi \quad (8b)$$

$$\leq 2\bar{\lambda}\psi^*\mathbf{P}(t)\psi = 2\bar{\lambda}V, \quad (8c)$$

where (8c) is obtained by the inequality in (7c). Integrating the inequality (8) over time t , we have

$$V(\psi, t) \leq e^{2\bar{\lambda}t}V(\psi, 0). \quad (9)$$

We then use the Rayleigh-Ritz theorem to obtain

$$\mu_{\min}[\mathbf{P}(t)]\psi^*\psi \leq V(\psi, t) \leq \mu_{\max}[\mathbf{P}(t)]\psi^*\psi, \quad (10)$$

where $\mu_{\min}[\cdot]$ and $\mu_{\max}[\cdot]$ represent the minimum and maximum eigenvalues of the argument. Combining the bound on $V(\psi, t)$ in (9) with (10) evaluated at $t = 0$, we obtain

$$\mu_{\min}[\mathbf{P}(t)]\|\psi(t)\|_2^2 \leq V(\psi, t) \quad (11a)$$

$$\leq e^{2\bar{\lambda}t}V(\psi, 0) \leq e^{2\bar{\lambda}t}\mu_{\max}[\mathbf{P}(0)]\|\psi(0)\|_2^2. \quad (11b)$$

Thus, we have

$$\|\psi(t)\|_2 \leq \sqrt{\frac{\mu_{\max}[\mathbf{P}(0)]}{\mu_{\min}[\mathbf{P}(t)]}}e^{\bar{\lambda}t}\|\psi(0)\|_2 \quad (12a)$$

$$\leq \sqrt{\frac{\mu_{\max}[\mathbf{P}(0)]}{\epsilon}}e^{\bar{\lambda}t}\|\psi(0)\|_2. \quad (12b)$$

Here, the inequality in (12b) is obtained by (7b). ■

We then discretize $\mathbf{P}(t)$ as $\mathbf{P}(t_i)$ and discretize $\mathbf{A}(t)$ as $\mathbf{A}(t_i)$, $i = 0, 1, \dots, n$ with a fixed time step $\Delta t = t_{i+1} - t_i$. The forward Euler method is used to approximate the time derivative as $\dot{\mathbf{P}}(t_i) = \frac{\mathbf{P}(t_{i+1}) - \mathbf{P}(t_i)}{\Delta t}$, which converts the LMI in (7) as:

$$\min \bar{\lambda} \quad (13a)$$

subject to $\mathbf{P}(t_i) \succeq \epsilon \mathbf{I}$, $\epsilon > 0$, $\forall i = 0, 1, \dots, n-1$, (13b)

$$\dot{\mathbf{P}}(t_i) + \mathbf{A}^*(t_i)\mathbf{P}(t_i) + \mathbf{P}(t_i)\mathbf{A}(t_i) - 2\bar{\lambda}\mathbf{P}(t_i) \preceq 0. \quad (13c)$$

For a time-periodic system, we can enforce periodicity on $\mathbf{P}(t)$ such that $\mathbf{P}(t_n) = \mathbf{P}(t_0)$ [13], [14], and we only need to consider one period for the discretized LMI. Thus, we select $t_0 = 0$ and $t_n = T$, where $T = \frac{2\pi}{\omega}$ is the oscillation period. We also found that using a time-invariant \mathbf{P} to construct a Lyapunov function candidate will result in the growth rate being overly conservative.

Because $\mathbf{A}(t)$ in (6) is a real matrix, we can assume the weighting matrix $\mathbf{P}(t) \in \mathbb{R}^{5 \times 5}$ and $\mathbf{P}(t_i) \in \mathbb{R}^{5 \times 5}$ as real symmetric matrices without loss of generality. The value of ϵ does not influence the upper bound of the growth rate $\bar{\lambda}$ due to the homogeneity of the constraints in (7c) and (13c), and thus, we set $\epsilon = 1$ without loss of generality. We use YALMIP [17] to formulate our LMI in (13) and use MOSEK [18] as the semi-definite programming (SDP) solver. We first check the stability of the system by checking the feasibility of constraints in (13) with $\bar{\lambda} = 0$, which is much quicker than calculating the value of $\bar{\lambda}$. If infeasible, we then solve (13) to minimize the upper bound of the growth rate $\bar{\lambda} > 0$ through bisection search over $\bar{\lambda}$.

B. Numerical simulation

The linear time-varying system in (5) was numerically integrated with `ode45` command in MATLAB for 50 periods, and we sample results $\psi(t)$ at a time step $\Delta t = \frac{50T}{2000}$. The non-dimensional perturbation energy in (14) was calculated for all times, which includes both the kinetic energy and the potential energy [4]:

$$e(t) = \frac{|\hat{u}|^2 + |\hat{v}|^2 + |\hat{w}|^2}{4} + \frac{Pr|\hat{S} - \hat{T}|^2}{4(R_p - 1)} \quad (14a)$$

$$=: \psi^*\mathbf{M}^*\mathbf{M}\psi, \quad (14b)$$

where

$$\mathbf{M} = \text{blkdiag} \left(\sqrt{\frac{\text{Pr}}{4(R_p - 1)}} \begin{bmatrix} -1 & 1 \end{bmatrix}, \frac{1}{2}, \frac{1}{2}, \frac{1}{2} \right). \quad (15)$$

Here, `blkdiag`(\cdot) means the block diagonal. This energy $e(t)$ can be connected to the vector norm $\|\psi\|_2$ based on the Rayleigh-Ritz theorem:

$$e(t) \leq \mu_{\max}[\mathbf{M}^*\mathbf{M}]\|\psi(t)\|_2^2. \quad (16)$$

To obtain the growth rate $\underline{\lambda}$ from numerical simulations, we then perform a least squares fit of $\ln(e)/2 = \underline{\lambda}t + B$ for the second half of the time series. We only fit the second half of the time series to avoid fitting the initial transient response. For each wavenumber pair, we conduct 50 simulations with initial conditions for each state variable $[\hat{T}, \hat{S}, \hat{u}, \hat{v}, \hat{w}]$ as a complex normally distributed random variable generated by `randn` command in MATLAB. We then compute the maximal growth rate from these 50 simulations. Fig. 2 shows sample results of $e(t)$ and the least squares fit associated with wavenumbers $(k, m_0) = (0.179, 3.01 \times 10^{-3})$.

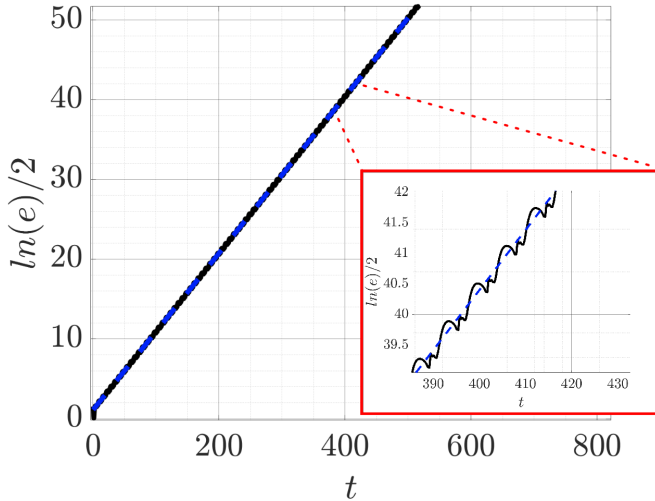


Fig. 2. $\ln(e)/2$ over t from numerical simulations (—) of system in (5) and a least squares fitted $\ln(e)/2 = \lambda t + B$ (—). The results are associated with wavenumbers $(k, m_0) = (0.179, 3.01 \times 10^{-3})$ and the initial condition producing the largest growth rate among 50 simulations with random initial conditions.

C. Floquet Theory

For a linear time-varying system, we have the solution as

$$\psi(t) = \Phi(t, t_0)\psi(t_0), \quad (17)$$

where $\Phi(t, t_0)$ is the state-transition matrix that satisfies

$$\partial_t \Phi(t, t_0) = \mathbf{A}(t)\Phi(t, t_0), \quad \Phi(t_0, t_0) = \mathbf{I} \quad (18)$$

with \mathbf{I} as the identity matrix. We can numerically approximate $\Phi(t, t_0)$ at $t = t_0 + n\Delta t$ as

$$\Phi(t_0 + n\Delta t, t_0) = \prod_{j=0}^{n-1} e^{\mathbf{A}(j\Delta t + t_0)\Delta t}. \quad (19)$$

Then, we compute Floquet multiplier $\gamma := \text{eig}[\Phi(T, 0)]$, where $\max |\gamma|$ represents the growth of solution norm over one period, i.e., $\frac{\|\psi(T)\|}{\|\psi(0)\|}$. Thus, we have the temporal growth rate predicted from the Floquet theory as $\lambda_F = \ln(\max |\gamma|)/T$.

IV. RESULTS

1) *Lyapunov Method Accurately Predicts the Growth Rate:* The growth rate of the linear time-varying system in (5) was computed over initial vertical wavenumbers $m_0 \in [0, 1.5]$ and x -direction wavenumbers $k \in [-0.5, 0.5]$ with uniformly sampled points $n_{\text{sample}} = 126$ in each wavenumber domain. Figs. 3a and 3b show $\bar{\lambda}$ obtained from the Lyapunov method in §III-A with temporal discretization points $n = 400$ and $n = 800$, respectively. For comparison, Fig. 3c shows λ obtained from numerical simulations in §III-B, and Fig. 3d shows λ_F obtained by the Floquet method in §III-C. In Fig. 3, the growth rate results with $\log_{10}(\lambda) < -4$ were truncated to $\log_{10}(\lambda) = -4$, which are shown as dark blue.

The general structure of the unstable parameter regime (“bulbs”) in each panel of Fig. 3 is consistent across these

three methods and also consistent with simulation results in Ref. [4]. There is a symmetry across the $k = 0$ axis with one main bulb followed by several thinner, elongated, and disconnected parameter regimes of instability. Small initial vertical wavenumbers m_0 generally resulted in the greatest instability. The width and height of the unstable parameter regime in Fig. 3a ($n = 400$) are slightly lower than those shown in Fig. 3b ($n = 800$). This indicates that the Lyapunov method requires large enough temporal discretization points n to predict the growth rate accurately. With increasing n , the Lyapunov method approached the results of numerical simulations (Fig. 3c) and the Floquet theory (Fig. 3d). We have also observed that the Lyapunov method with drastic under-sampling on the order of $n \sim 10^1$ can lose entirely the instability pattern of $\bar{\lambda}(k, m_0)$.

Table II shows the maximal growth rate over (k, m_0) parameter regimes in Fig. 3 and the corresponding (k, m_0) wavenumber pair for these three methods. The maximal growth rate predicted from the Lyapunov method is approaching that obtained from the numerical simulations ($\log_{10}[\lambda] = -1.00754$) and the Floquet theory ($\log_{10}[\lambda_F] = -1.00765$). Moreover, the wavenumber pair associated with the maximal growth rate is $(k, m_0) = (0.180, 0.000)$ for the Lyapunov method with $n = 800$, which agrees well with that obtained from numerical simulations and the Floquet theory.

Method	n	$\log_{10}(\lambda_{\max})$	(k, m_0) pair
Lyapunov	400	-1.01807	(0.172, 0.000)
	800	-1.01316	(0.180, 0.000)
Simulations	—	-1.00754	(0.180, 0.000)
Floquet	2000	-1.00765	(0.180, 0.000)

TABLE II. Maximum growth rate and the associated wavenumber pair (k, m_0) obtained by three different stability analysis methods.

Fig. 4 then investigates the convergence of the Lyapunov method and Floquet theory by plotting the growth rate as a function of n , and we use the growth rate computed from numerical simulations (—) as a basis for comparison. As the number of temporal discretization points increases, Fig. 4 shows that the growth rate predicted by the Lyapunov method (—) and the Floquet theory (···) both converge to the growth rate obtained by numerical simulations (—), while Floquet theory converges faster than the Lyapunov method.

2) *Eigendecomposition of $\mathbf{P}(t)$ Provides Insights into Time-dependent Instabilities:* Here, we perform an eigendecomposition of $\mathbf{P}(t)$ obtained from the Lyapunov method to provide insights into the instantaneous growth rate and principal axes of instability. The eigendecomposition $\mathbf{P}(t) = \mathbf{Q}(t)\mathbf{\Lambda}(t)\mathbf{Q}(t)^{-1}$ at each time t was performed using the `eigenshuffle` routine [19] to ensure continuity and consistency of eigenvectors and eigenvalues over time. This eigendecomposition was performed on the $\mathbf{P}(t)$ corresponding to $n = 2000$ and the wavenumber pair $(k, m_0) = (0.179, 3 \times 10^{-3})$. Fig. 5a shows the largest two eigenvalues μ_1 and μ_2 of $\mathbf{P}(t)$, while other eigenvalues (not shown) have much smaller magnitudes. The peak $\mu_1[\mathbf{P}(t)]$ aligns closely with the peak strength of the background shear flow $A_U(t)$, resulting in the time-dependent instability having

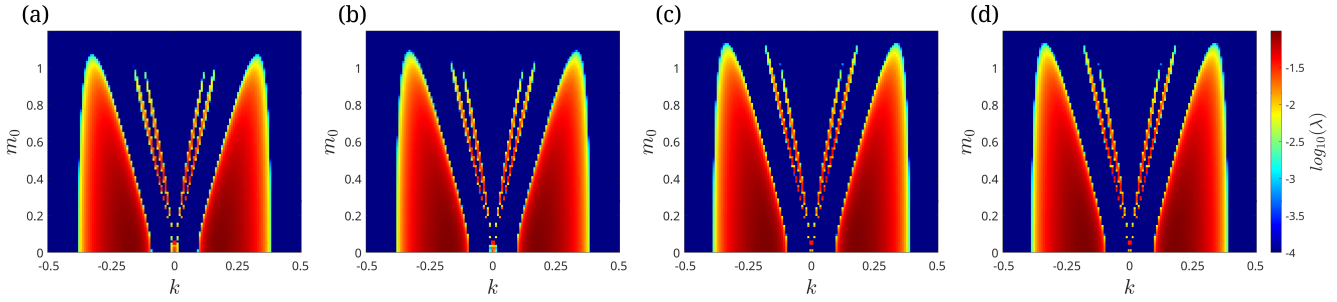


Fig. 3. Stability analysis of the linear time-varying system in (5) over different (k, m_0) using three different methods in §III. (a) $\log_{10}(\bar{\lambda})$ using the Lyapunov method in §III-A with $n = 400$, (b) $\log_{10}(\bar{\lambda})$ using the Lyapunov method in §III-A with $n = 800$, (c) $\log_{10}(\bar{\lambda})$ using numerical simulations as described in Section III-B, and (d) $\log_{10}(\lambda_F)$ using the Floquet theory in §III-C with $n = 2000$.

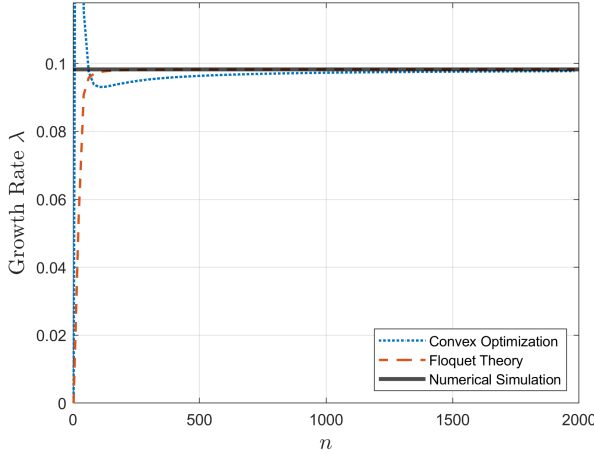


Fig. 4. The convergence of the Lyapunov method and the Floquet theory for $(k, m_0) = (0.179, 3 \times 10^{-3})$ as increasing n , the number of the temporal discretization points. The thick black line shows the growth rate obtained by numerical simulations in §III-B.

roughly half the period of the background shear flow. The maximal magnitude of background shear flow occurs at $t = 6.283, 12.566$, while the peak of $\mu_1[\mathbf{P}(t)]$ occurs at $t_{\text{peak},1} = 5.569$ and $t_{\text{peak},2} = 11.862$. Fig. 5b then shows each component of the eigenvector associated with $\mu_1[\mathbf{P}(t)]$. The v velocity component is zero for all time since a 2D model was studied (i.e., $l = A_V(t) = 0$), and the u velocity component was also negligible. As the peak of $\mu_1[\mathbf{P}(t)]$ is approached, temperature increasingly drives instability, while salinity diminishes marginally. At the steep drop-off of $\mu_1[\mathbf{P}(t)]$, temperature is the dominant factor, while the salinity will change sign. During non-peak times, salinity almost exclusively influences the instability.

3) Computational Resources Requirement of the Lyapunov Method: We also test the memory usage and running time for the Lyapunov method as summarized in Table III. Here, we parallelize the computation in the k parameter regime and use one computing node with 126 cores and 500 GB of RAM at UConn Storrs High Performance Computing (HPC) facility to generate results in Fig. 3. We take $n_{\text{sample}} = 126$ samples in both k and m_0 parameter regimes. As the number of temporal discretization points n increases, the computational

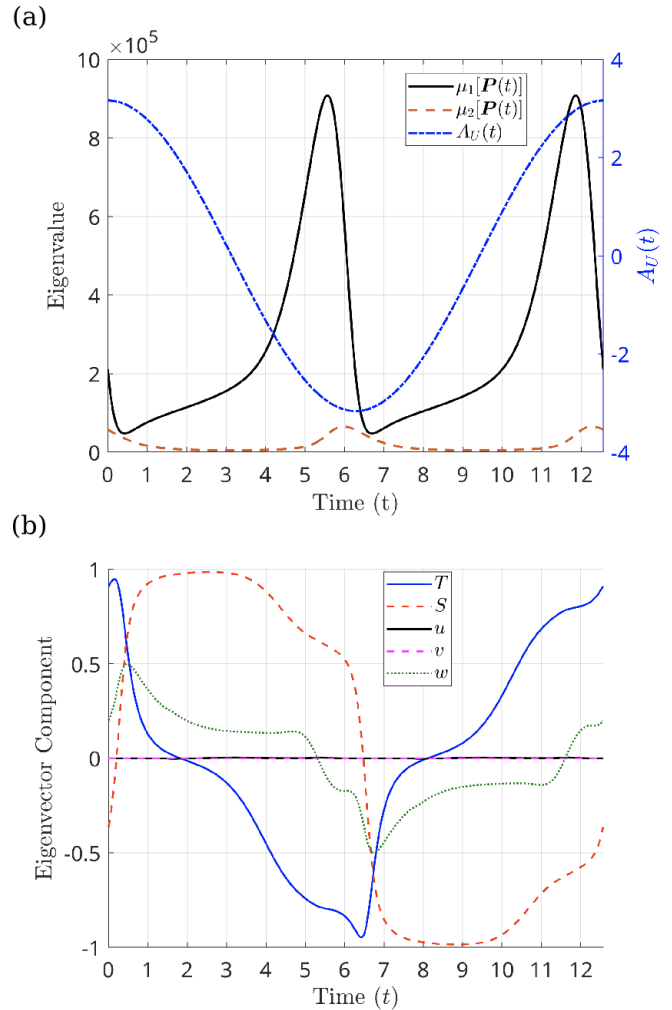


Fig. 5. Eigendecomposition of $\mathbf{P}(t)$ obtained from the Lyapunov method for $(k, m_0) = (0.179, 3 \times 10^{-3})$ with $n = 2000$. (a) The two largest eigenvalues $\mu_1[\mathbf{P}(t)]$ and $\mu_2[\mathbf{P}(t)]$ over time with the background shear flow $A_U(t)$. (b) Eigenvector components corresponding to the dominant eigenvalue over time. Note that u and v components are nearly zero.

time and memory requirements of the Lyapunov method increase as a result of the increased number of constraints. The CPU hours increase much faster than the memory usage as we are increasing the number of temporal discretization points n . Note that the time per (k, m_0) and the memory per CPU are estimates of the average usage across all CPUs, whether or not they were idle. Because we do not solve the growth rate $\bar{\lambda}$ for the stable case if the constraints in (13) are feasible with $\bar{\lambda} = 0$ (i.e., the system is stable), idle CPUs could have occurred if their allotted work contains more stable parameter regimes than other CPUs. We also report the computational resources required for numerical simulations and the Floquet theory in Tab. III. Here, we found numerical simulations (with 50 random initial conditions) require computational time similar to the Lyapunov method with $n \in [200, 400]$, while the Floquet theory will be much faster than the Lyapunov method.

Method	n	Max Mem. Usage (GB)	Mem. per CPU (GB)	CPU Hours	Time per (k, m_0) (s)
Lyapunov	200	244.5	1.94	235	53.2
	400	332.4	2.63	693	157
	600	328.1	2.60	1638	371.5
	800	354.3	2.81	2685	690
Simulations	—	196.1	1.56	464.7	105
Floquet	2000	187.4	1.49	5.04	1.14

TABLE III. HPC performance while evaluating the growth rate for each method corresponding to Fig. 3. The maximal memory usage and CPU hours are for the computation of $n_{\text{sample}} = 126$ horizontal wavenumber k and $n_{\text{sample}} = 126$ initial vertical wavenumber m_0 . We parallelize the code in the k parameter regime with 126 cores. Performance of numerical simulation is associated with 50 random initial conditions.

Although Floquet theory is much more computationally efficient, it is limited to analyzing linear time-periodic systems. Numerical simulations, in principle, cannot prove stability, but only provide results for certain initial conditions to support the stability prediction. For nonlinear systems, extensive simulations (e.g., 100,000 simulations with random initial conditions [11]) are required to fully characterize the region of attraction. The Lyapunov method, instead, can rigorously certify the region of attraction for nonlinear systems without extensive simulations (e.g., Ref. [15]) and can be generalized to non-periodically time-varying systems (e.g., Ref. [16]). This work serves as a first step to demonstrate that the Lyapunov approach can predict the growth rate consistent with numerical simulations and Floquet theory for *linear time-periodic* systems. Our ongoing work will generalize this Lyapunov-type framework to analyze *nonlinear non-periodically* time-varying systems.

V. CONCLUSION AND FUTURE WORK

We demonstrated that the Lyapunov method is a viable tool to identify instabilities for a linear time-periodic system describing thermohaline convection with a periodically time-

varying background shear flow. In the linear matrix inequalities formulation, we include the time derivative of the weighting matrix $\dot{P}(t)$ of the Lyapunov function candidate, which is approximated by the forward Euler method. With enough temporal discretization points, we find that the growth rate predicted by the Lyapunov method or the Floquet theory converges to that obtained by numerical simulations. The eigenvectors of the weighting matrix $P(t)$ are employed to uncover the instantaneous principal direction of instabilities.

We also benchmark the memory and computational time required by the Lyapunov method and how it varies over the number of temporal discretization points, which suggests future directions for improving the computational efficiency of the Lyapunov method. Another future direction is to explore high-order finite difference methods to approximate $\dot{P}(t)$, which might help improve the convergence of the Lyapunov method. The Lyapunov method can be further extended to study the nonlinear stability and systems with non-periodic time dependence; see e.g., Ref. [16].

REFERENCES

- [1] M. H. Alford, J. A. MacKinnon, H. L. Simmons, and J. D. Nash, “Near-inertial internal gravity waves in the ocean,” *Annu. Rev. Mar. Science*, vol. 8, pp. 95–123, 2016.
- [2] B. R. Sutherland, *Internal gravity waves*. Cambridge university press, 2010.
- [3] P. Washam, K. W. Nicholls, A. Münchow, and L. Padman, “Tidal modulation of buoyant flow and basal melt beneath Petermann Gletscher Ice Shelf, Greenland,” *J. Geophys. Res.: Oceans*, vol. 125, p. e2020JC016427, 2020.
- [4] T. Radko, “Thermohaline-shear instability,” *Geophys. Res. Lett.*, vol. 46, pp. 822–832, 2019.
- [5] ———, “Instabilities of a time-dependent shear flow,” *J. Phys. Oceanogr.*, vol. 49, pp. 2377–2392, 2019.
- [6] M. D. Graham and D. Floryan, “Exact coherent states and the nonlinear dynamics of wall-bounded turbulent flows,” *Annu. Rev. Fluid Mech.*, vol. 53, pp. 227–253, 2021.
- [7] S. H. Davis, “The stability of time-periodic flows,” *Annu. Rev. Fluid Mech.*, vol. 8, pp. 57–74, 1976.
- [8] H. K. Khalil, *Nonlinear systems*. Upper Saddle River, 2002.
- [9] E. Knobloch and R. Krechetnikov, “Stability on time-dependent domains,” *J. Nonlinear Sci.*, vol. 24, pp. 493–523, 2014.
- [10] G. Floquet, “Sur les équations différentielles linéaires à coefficients périodiques,” in *Ann. Sci. Ec. Norm. Super.*, vol. 12, 1883, pp. 47–88.
- [11] M. Joglekar, U. Feudel, and J. A. Yorke, “Geometry of the edge of chaos in a low-dimensional turbulent shear flow model,” *Phys. Rev. E*, vol. 91, p. 052903, 2015.
- [12] S. Boyd, L. El Ghaoui, E. Feron, and V. Balakrishnan, *Linear Matrix Inequalities in System and Control Theory*. Society for Industrial and Applied Mathematics, 1994.
- [13] C. Böhm, M. Lazar, and F. Allgöwer, “Stability of periodically time-varying systems: Periodic Lyapunov functions,” *Automatica*, vol. 48, pp. 2663–2669, 2012.
- [14] B. Zhou and G.-R. Duan, “Periodic Lyapunov equation based approaches to the stabilization of continuous-time periodic linear systems,” *IEEE Trans. Autom. Control*, vol. 57, pp. 2139–2146, 2011.
- [15] C. Liu and D. F. Gayme, “Input-output inspired method for permissible perturbation amplitude of transitional wall-bounded shear flows,” *Phys. Rev. E*, vol. 102, p. 063108, 2020.
- [16] Z. Wei, W. Zhao, and C. Liu, “Upper bound of transient growth in accelerating and decelerating wall-driven flows using the Lyapunov method,” *arXiv preprint arXiv:2508.01410*, 2025.
- [17] J. Lofberg, “YALMIP: A toolbox for modeling and optimization in MATLAB,” in *Proceedings of the IEEE International Conference on Robotics and Automation*, vol. 3, 2004, pp. 284–289.
- [18] MOSEK ApS, *The MOSEK optimization toolbox for MATLAB manual*, 2024.
- [19] J. D’Errico. Eigenshuffle. [Online]. Available: <https://www.mathworks.com/matlabcentral/fileexchange/22885-eigenshuffle>